Characterizing sub-pixel Landsat ETM+ fire severity on experimental fires in the Kruger National Park, South Africa

T. Landmann*

Burn severity was quantitatively mapped using a unique linear spectral mixture model to determine sub-pixel abundances of different ashes and combustion completeness measured on the corresponding fire-affected pixels in Landsat data. A new burn severity index was derived that is shown to map three categories of burn severity on three experimental burn plots in the southern Kruger National Park, South Africa. Those pixels which corresponded to a greater abundance of white ash were found to be significantly related to the pre-burn above-ground fuel biomass and an indicator of burn efficiency. Landsat ETM+ combustion completeness was most significantly related to the abundance of post-burn residual, non-photosynthetic fuel biomass. For the same reflectance change in pre- and post-fire imagery, a greater magnitude of fire severity was measured on corresponding ETM+ pixels. This implies that fire severity depends more on the colour of the ash than on the magnitude of change in reflectance. Burned area mapping methods that rely on reflectance change in multi-temporal imagery may not reliably characterize burn effects such as fire severity and efficiency in semi-arid savannas.

Introduction

Satellite imagery provides accurate information on fires over large or remote areas where direct characterization of fires cannot be feasibly measured or observed by resource managers in the field. Remote-sensing methods use parts of the electromagnetic spectrum not visible to the eye to extract a wide range of fire-related information.[1,2]

Fire severity in remote sensing is defined as the degree or magnitude of vegetation change induced by fire. It is usually inferred from the date and pattern of mapped burned areas.[2] In ecological terms, fire severity is the extent of physical, biological and chemical changes at a site.[3] This includes the fire effect on the recovery of individual species and different vegetation components as well as the downward fire heat flux and its effect on soil and plant interactions.[3-6]

Changes in fire severity result in an altered ecological impact within a vegetation biome, thus modifying ecosystem composition and functioning.[2,5,7] Spatially explicit information on fire severity is required by reserve or resource managers for monitoring the ecological effects of fires and biodiversity patterns.[8,9] The information can be used to assess the current fire situation of a managed region, and areas that are deviating from the intended fire policy can be identified.[2] For instance, resource managers may require complete and severe fires to suppress a woody savanna component in favour of a grass sward.[4] Spatial information on fire severity can also help locate areas that need erosion mitigation studies or provide local emission models with data on the fraction of fuel mass consumed.

Remote-sensing methods that quantitatively map fire severity in savannas over large, phenologically diverse regions are still not reliable or readily available for post-fire assessments. In the last decade, 'image classification' methods used mainly principal component analyses, vegetation indices, or linear transformation techniques to map ordinal classes of severity in Landsat data.[10-12] The remote-sensing information was combined with field data on vegetation and soil heat penetration criteria.[12-14]

In this paper, a burn severity index (BSI) (unitless) is derived from multi-temporal sub-pixel combustion completeness (CC) data and a unique linear mixture model. The spectral endmembers for the unmixing calculation were derived from an Analytical Spectral Device (ASD) radiometer. Endmembers represent the purest 'homogeneous' materials; other materials represent mixtures of endmembers.[15] Spectral mixing results are related to available fuel biomass (based on dry matter weight) calculated from Landsat Enhanced Thematic Mapper (ETM+) Tasselled Cap reflectance.[16,17] Combustion completeness calculations were derived from a recent study that found a significant relationship between Landsat ETM+ near-infrared reflectance and CC field measurements.[18] The only other study known to use spectral mixing models in estimating fire severity at a Landsat sub-pixel scale is that of Rogan and Franklin[3] in southern California.

Methods

Data acquisition

Two Landsat ETM+ cloud-free datasets (ETM+ path 168, row 077) captured over Skukuza, Kruger National Park (KNP) on 12 June 2000 and 15 August 2000 were investigated to derive pre-fire fuel biomass (in units of g m^{-2}), capture the burned area, and predict CC for each of the Landsat ETM+ pixels corresponding to fire. The Landsat data were corrected to at-sensor reflectance and surface reflection using an atmospheric radiative transfer model, as described by Roy and Landmann.[18,19] Surface reflection is needed to make Landsat data comparable to the at-nadir reflectance of spectral endmembers.

A 9-pixel Landsat ETM+ sampling area was investigated on each of three experimental burn plots (EBPs) in the Kambeni area of the KNP. The burn plots are part of a long-term burning experiment begun in the park in 1954.[20]

The pixel grids were determined to be homogeneous in their physiognomic and primary vegetation structure and in their morphological topography features, based on field work conducted in August 2000.[18] The 9-pixel grid was located well within each plot in order to exclude edge effects.

Above-ground fuel biomass available for burning was calculated (per pixel) from Landsat ETM+ Tasselled Cap (at-sensor) reflectance, according to a study conducted on the same EBPs in 2000.[16] The Landsat Tasselled Cap pixel data were selected from the field corresponding to a 9-pixel filter. The three sample EBPs were burnt on the morning of 14 August 2000 under the same micrometrological conditions; and they were noted to be homogeneously burnt.

After the fire, 500 g of pure white ash, 500 g of representative black ash and over 1 kg of residual non-photosynthetic fuel biomass (senescent grass, twigs, leaves and bark) samples were collected. The samples were analysed in the laboratory to determine their multi-spectral reflectance using an ASD radiometer, which measures spectral reflectance in the range 0.45–2.2 μm at intervals of 0.01 μm. Spectral endmembers of black ash, white ash and non-photosynthetic vegetation were derived from the ASD spectral information and re-sampled to wavelengths

*CSIR Environmentek, P.O. Box 395, Pretoria 0001, South Africa, and Department of Landscape Ecology, University of Göttingen, Germany. E-mail: tlandmann@csir.co.za

simulating (at-nadir) Landsat ETM+ reflectance in the six reflective bands.

Combustion completeness was derived for the same pixel filter from geo-located Landsat ETM+ reflectance using the near infrared (NIR) wavelength (0.841–0.876 μm). A difference index was used for the pre- and post-burn fire reflectances and related to the fraction of fuel actually combusted on the EBPs.[18]

Ash endmember modelling

Landsat ETM+ re-sampled ash reflection spectra from 0.41 μm to 2.11 μm were simulated from ASD radiometer measurements (Fig. 1). Ash spectral curves for different white ash percentage abundances were interpolated between the 100% white ash and the black ash endmembers, as collected in the field. By dividing the sampled black ash spectra by the white ASD ash spectral endmember (also called the reference endmember), the relative abundance of the pure white ash spectra in black ash was determined as being 9%.[21] The different ash spectra can be used to simulate, in theory, 'grey' ash levels corresponding to different levels of emitted energy over longer burning periods, that is, combustion efficiency. Combustion efficiency is defined as the degree of oxidation of the fuel (proportion of carbon oxidized as CO_2).[22]

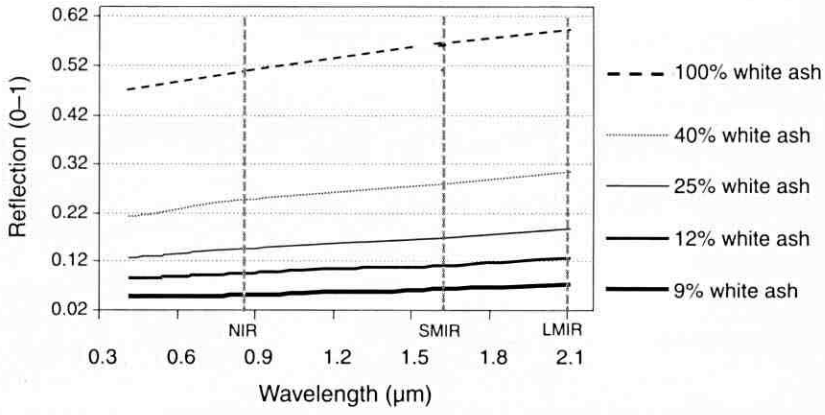

Fig. 1. Spectral ash reflectance curves that simulate different percentage white ash contents in 'grey' ash in the range from 0.45 μm to 2.2 μm. The bottom (black) curve corresponds to the reflection of the black ash as collected in the field and contains 9% white ash. The positions of narrow-band Landsat ETM+ near-infrared (NIR), short middle infrared (SMIR) and long middle infrared (LMIR) bands are marked with broken vertical lines.

Linear spectral unmixing

Linear spectral unmixing was performed using Landsat ETM+ data for the three Kambeni EBPs. Linear spectral unmixing assumes that a Landsat fire-affected pixel is a multivariate product of several spectral (physically pure) components.[23] This implies that for a given pixel the multi-spectral signal (X) can be described as the sum of the linear function of ground-cover proportions from the spectrally pure endmembers matrix (M_i) and for the pixel component i. The abundance of a material is therefore defined as $(1 - x)$, where

$$X = \Sigma M_i f + \epsilon. \quad (1)$$

The term f is the fractional abundance vector of the known endmember matrix (M). ϵ is the random term used to describe residual atmospheric or instrument noise. All fractional abundances are in proportions between zero and one.[24]

The physical validity of the unmixing result depends critically on the choice of possible candidate endmembers. The validity can be assessed by analysing the abundance fraction (f) and the root mean square error.[23] Endmembers can also be directly extracted from the image itself as being 'pure' representatives of a certain landscape feature or pixel component.[25] Several linear unmixing trial calculations using different endmember combinations were investigated for their validity. The following endmembers were selected: non-photosynthetic (or 'brown') vegetation (derived from the ASD measurements), photosynthetic (or 'green') vegetation (extracted from the image itself), 9% white in black ash curve, and 12% white in black ash (or the 'grey' ash) curve.

Endmember combinations using the soil endmember, together with the brown vegetation endmember, and the shadow with the photosynthetic (green) vegetation endmember did not yield meaningful results. This has been observed previously in other studies and may be due to spectral similarities between bare soil surfaces and brown vegetation. Similarly, multiple reflectance scattering in tree canopies may cause confusion between photosynthetic leaf biomass and shadow.[24,25]

Results and discussion

Landsat-estimated pre-fire fuel mass (in units of g m^{-2}) is significantly related to the abundance of grey ash $(1 - x)$ from the spectral unmixing result (R^2 = 0.49, P = 0.001) (Fig. 2). No relationship was found between black ash abundances and pre-fire biomass. Since fuel biomass is an important determinant of fire severity,[4,10] and more severe and efficient fires produce whiter ash,[18,26] most pixels relating to Kambeni 5 can be classified as corresponding to a severe burn.

Landsat ETM+ CC (using ETM+ band 4) was used as a second independent data source to study the relationship between ash colour and fire severity. The relationship (R^2) between grey ash abundance and Landsat CC exhibited a value of 0.46 ($P < 0.001$). No significant relationship was found for black ash as a function of CC. The abundance of unburnt brown vegetation from the unmixing result correlated significantly with Landsat ETM+ CC ($R^2 = 0.73$, $P < 0.002$) (Fig. 3). This implies that CC is a good measure for determining the proportion of fuel biomass consumed by fire and of relative fire impact.

Fire severity mapping

Fire severity is defined as the degree of change caused by a fire event.[1,8] Burn severity can be characterized as the product of the abundance of the grey ash endmember, $M_A f_{(1-x)}$, from spectral unmixing and CC of the same area unit or pixel:

$$\text{BSI} = M_A f_{(1-x)} \times \text{CC}, \quad (2)$$

where BSI is the burn severity index.

The variables in (2) describe different fire severity effects. Grey ash $M_A f_{(1-x)}$ is related to the heat of combustion (in units of kJ kg^{-1}) and pre-fire fuel biomass. CC is a measure of the fraction of brown fuel biomass that is consumed (that is, the relative fire impact), irrespective of the heat of combustion and pre-fire fuel quantity. More intense fires (in units of kJ s^{-1} m^{-1}) usually produce less whitish ash in flaming combustion.[27] Conversely, more efficient fires usually emit heat over longer periods as they have a prolonged smouldering combustion phase.[28]

Figure 4 illustrates the magnitude of response of the BSI as a (non-linear) function of reflection change in pre- and post-fire imagery for the three EBPs (R^2 = 0.52, $P < 0.001$). The shape of the curve shows that the BSI values depend more on ash colour (that is, burn efficiency) than on CC, as the latter is essentially determined by the change in reflection (ρ), i.e. pre-burn$_\rho$ – post-burn$_\rho$.

Characterizing fire severity or mapping fire effects using

21. Hill J. (1990). Neue Wege zur geowissenschaftlichen Interpretation multispektraler Fernerkundungsdaten. *Geogr. Rundschau* **50**, 113–119.
22. Ward D.E., Hao W.M, Susott R.A., Babbitt R.E., Shea R.W., Kauffman J.B. and Justice C.O. (1996). Effect of fuel composition on combustion efficiency and emission factors for African savanna ecosystems. *J. Geophys. Res.* **101**, 23569–23576.
23. Elmore A.J., Mustard J.F., Manning S.J. and Lobell D.B. (2000). Quantifying vegetation change in semiarid environments: precision an accuracy of spectral mixture analysis and the Normalized Difference Vegetation Index. *Remote Sens. Environ.* **73**, 87–102.
24. Settle J. and Campbell N. (1998). On the errors of two estimators of sub-pixel fractional cover when mixing is linear. *IEEE Trans. Geosci. Remote Sens.* **36**, 163–170.
25. Roberts D.A., Green R.O. and Adams J.B. (1993). Discriminating green vegetation, non-photosynthetic vegetation and soils in AVIRIS data. *Remote Sens. Environ.* **44**, 255–270.
26. Stronach N.R.H and McNaughton S.J. (1989). Grassland fire dynamics in the Serengeti Ecosystem and a potential method of retrospective estimating fire energy. *J. Appl. Ecol.* **26**, 1025–1033
27. Trollope W.S.W. and Trollope L.A. (2002). Fire behavior: a key factor in the fire ecology of African grasslands and savannas. In *Forest Fire Research & Wildland Fire Safety*, pp. 1–15. Millpress, Rotterdam.
28. Ward D.E. and Radke L.F. (1993). Emission measurements from vegetation fires: a comparative evaluation of methods and results. In *Fire in the Environment: The Ecological, Atmospheric, and Climatic Importance of Vegetation Fires*, eds P.J. Crutzen and J.G. Goldammer, pp. 53–76. John Wiley, New York.
29. Swap R.J., Annegarn H.J. and Otter L. (2002). Southern African Regional Science Initiative (SAFARI 2000): summary of science plan. *S. Afr. J. Sci.* **98**, 119–124.

Relationships between diffuse and global solar radiation in southern Africa

M. Tsubo*† and S. Walker*

Diffuse solar radiation, which is not routinely measured at weather stations, has been estimated empirically, from global solar radiation, around the world but not in southern Africa. We report here empirical relationships describing the components of solar radiation at eight locations throughout the subcontinent. Data on diffuse and global solar radiation were collected at weather stations, at latitudes between 22° and 34°S and at altitudes from 0 to 1725 m, representing various climate zones. A simple linear equation is proposed relating the ratio of diffuse to global solar radiation to the ratio of global to extraterrestrial solar radiation for the subcontinent, including both semi-arid/arid and warm temperate climate zones.

The diffuse solar radiation model

In crop modelling as well as in solar engineering, it may be necessary to separate global solar radiation into its diffuse and direct components. The method used to estimate global solar radiation at the earth's surface is divided broadly into two approaches: the Beer's (Bouguer-Lambert's) Law model and the Liu and Jordan (regression) model.[1] The former estimates direct solar radiation whereas the latter allows diffuse solar radiation to be calculated. Beer's Law describes the attenuation of monochromatic radiation through the atmosphere. The transmittance of direct radiation from the top of the atmosphere to the earth's surface is described by an exponential equation involving the product of the atmospheric extinction coefficient and air mass. The atmospheric extinction coefficient is subdivided into terms that describe Rayleigh scattering and Mie scattering and absorption by ozone, water vapour and other gas coefficients. The atmospheric extinction coefficient is therefore complex. By contrast, the Liu and Jordan model is a simple equation; that is, the ratio of diffuse to global solar radiation (K) can be estimated from the clearness index, defined as the ratio of global to extraterrestrial solar radiation (K_T). Researchers have found relationships between K and K_T at several locations on an hourly, a daily or a monthly basis.[2–5] Little information concerning the diffuse Liu and Jordan model is, however, available for southern Africa and the southern hemisphere. The objective of this study was, therefore, to investigate relationships between K and K_T on an hourly basis throughout southern Africa.

*Department of Soil, Crop and Climate Sciences, University of the Free State, P.O. Box 339, Bloemfontein 9300, South Africa.
†Author for correspondence. E-mail: tsubom@sci.uovs.ac.za

Methods

Hourly global and diffuse solar radiation (0.3–2.8 μm wavelength) data for eight southern African weather stations, including Windhoek (22°34'S, 17°06'E, 1725 m, Köppen climate classification: Bsh), Pretoria (25°44'S, 28°11'E, 1330 m, Cwb), Keetmanshoop (26°34'S, 18°07'E, 1066 m, Bwk), Bloemfontein (29°06'S, 26°18'E, 1351 m, Bsk), Durban (29°58'S, 30°57'E, 8 m, Cfa), Middelburg (31°29'S, 25°02'E, 1270 m, Bsk), Cape Town (33°58'S, 18°36'E, 44 m, Csb) and Port Elizabeth (33°59'S, 25°36'E, 60m, Cfb), were provided by the South African Weather Service. All radiation measurements were taken using Kipp and Zonen CM3 or CM5 thermopile pyranometers (Kipp & Zonen, Delft, The Netherlands). The period of the data sets varied from 24 to 41 years between 1957 and 1997. Daily extraterrestrial solar radiation on a horizontal surface was calculated using the sun–earth geometry relationship.[6] Variations in total solar irradiance have been observed above the atmosphere by satellite.[7] However, the 11-year solar activity cycle was assumed to have no effect on total solar irradiance because the accuracy of the satellite measurements (± 0.2 %) is greater than the solar irradiance variations (± 0.1 %).[8] In this study, therefore, a constant value of 1373 W m^{-2} was taken as the solar constant.[9]

Results and discussion

Previous studies involving diffuse solar radiation models classified K in terms of K_T over various ranges.[2–5] Those classes are: (i) the low K_T class, (ii) the middle K_T class and (iii) the high K_T class. In general, the diffuse fraction of solar radiation in the high K_T class is small. By contrast, the diffuse fraction of solar radiation in the low K_T class is high. These classes serve also to describe sky conditions and solar angles; that is, the high K_T class means clear sky and/or high solar elevation, whereas the low K_T class describes overcast sky and/or low solar elevation. Various factors affect the relationship between K and K_T. The maximum K_T in the southern hemisphere (0.77–0.82 for Australia) is higher than that in the northern hemisphere (0.70–0.75).[5] This difference may be explained by the enhanced aerosol content of the atmosphere in the northern hemisphere due to the greater land area and pollution load.[5] The relationship may also be dependent on latitude,[4] as well as on differences in atmospheric conditions, especially water content of the atmosphere and cloud type.[10] In our study, most of the data were distributed over the K_T range between 0.2 and 0.8 (the middle class) whereas the other ranges (the low K_T class: $0.0 \leq K_T < 0.2$ and the high K_T class: $0.8 < K_T \leq 1.0$) were less well represented. An average value of K in each K_T class was taken year by year [sample size was the number of years, means and standard errors of K were also calculated (Table 1)]. Average K values for the semi-arid/arid climate zone (represented by Windhoek, Keetmanshoop, Bloemfontein and Middelburg) were 0.887, 0.348 and 0.136 in the low, middle and high K_T classes,

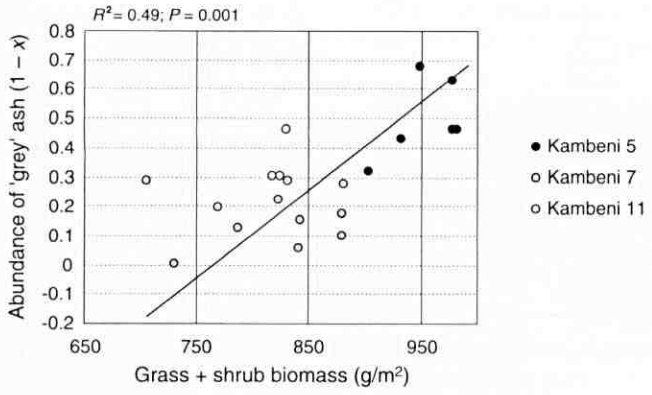

Fig. 2. Abundances of grey ash (1 – x) in Landsat ETM+ data and Landsat ETM+ modelled pre-fire biomass fuel loads (g m^{-2}) for the sample experimental burn plots. The pre-fire image was acquired on 12 June 2000 and used to derive the pre-burn biomass using Landsat ETM+ Tasselled Cap index data.

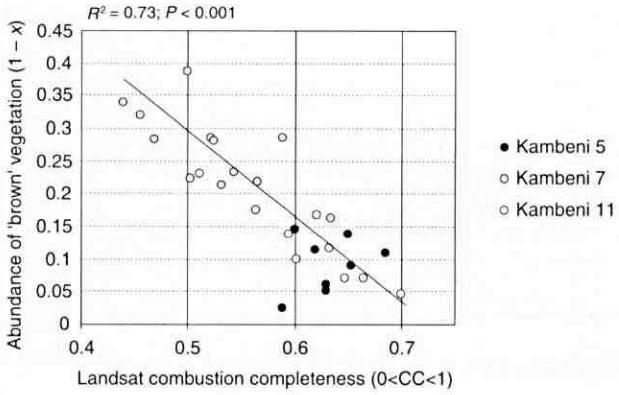

Fig. 3. Relationship between residual non-photosynthetic (brown) vegetation abundance (1 – x) from linear unmixing and Landsat ETM+ CC (using the NIR wavelength).

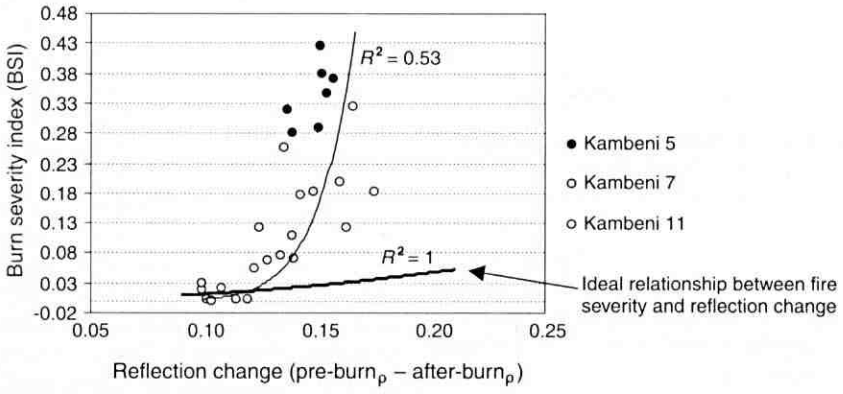

Fig. 4. Burn severity index (BSI) as a function of Landsat ETM+ absolute reflection change (pre-burn$_\rho$ – after-burn$_\rho$) using the NIR wavelength band (R^2 = 0.53). The ideal relationship (R^2 = 1) between reflection change and the BSI is also shown.

change in reflectance between images may therefore not be feasible because fires with the same change in reflectance show considerable differences in fire severity. This has implications for fire mapping methods that quantify fire extent or severity and rely on the maximum reflectance change between pre- and post-fire imagery as a surrogate for fire effects.

The BSI levels can further be used to derive continuous BSI classes. Kambeni 5, for example, can be classified as being affected by a severe fire. Kambeni 11 can be classed as a moderate fire, and most pixels in Kambeni 7 can be classified as corresponding to a low severity burn.

This work was conducted as part of the SAFARI 2000 Regional Science Initiative.[29] Field assistance was provided by the Kruger National Park staff, in particular Andre Potgieter of Scientific Services. Funding for this research came primarily from the Gottlieb Daimler and Karl-Benz Foundation, the University of Göttingen and NASA's Land Use and Land Cover Change programme. I am especially grateful to the CSIR for hosting the research activities, and in particular to Bob Scholes.

Received 5 November 2002. Accepted 2 June 2003.

1. White J.D., Ryan K.C., Key C.C.and Running S.W. (1996). Remote sensing of forest fire severity and vegetation recovery. *Int. J. Wildl. Fire.* **6**, 125–136.
2. Flasse S.P., Trigg S.N., Ceccato P.N., Perryman A.H., Hudak A.T., Thompson M.W., Brockett B.H., Drame M., Ntabeni T., Frost P.E., Landmann T. and le Roux J.L. (in press). Remote sensing of vegetation fires and its contribution to a management fire information system. In *Fire Management Handbook for Sub-Saharan Africa*, eds J.G. Goldammer and N.C. de Ronde. BBP Academic, The Hague.
3. Rogan J. and Franklin J. (2001). Mapping burn severity in southern California using spectral unmixing analysis. In *Proc. International Geoscience and Remote Sensing Symposium (IGARRS '01)*, Sydney, Australia.
4. Trollope W.S.W. and Tainton N.M. (1986). Effect of fire intensity on the grass and bush components of the Eastern Cape Thornveld. *J. Grassland Soc. Sthn Afr.* **2**, 27–42.
5. Michalek J.L., Colwell J.E., French N.H.F., Kasischke E.S., Johnson R.D. (2000). Using Landsat TM data to estimate carbon release from burned biomass in an Alaskan spruce forest complex. *Int. J. Remote Sens.* **21**, 329–343.
6. Yokelson R.J., Susott R.A., Babbitt R.E., Ward D.E. and Hao W.M. (1999). Trace gas emissions from specific biomass fire-types. In *START Synthesis Workshop on Greenhouse Gas Emission, Aerosols and Land Use and Cover Change in* Southeast Asia, ed. T. Moya, SARCS, IGAC, LUCC, IGBP, pp. 329–343. China-Tapei, Taipei.
7. Kaufman Y. and Justice C.O. (1998). Algorithm Technical Background Document: MODIS Fire Product. EOS ID no. 2741.
8. Chaffey C.J. and Grant C.D. (2000). Fire management implications of fuel loads and vegetation structure in rehabilitated sand mines near Newcastle, Australia. *J. For. Ecol. Mngmnt* **129**, 269–278.
9. Caetano M.S.R., Mertes L., Cadete L. and Pereira J.M.C. (1995). Assessment of AVHRR data for characterizing burned areas and post-fire vegetation recovery. In *Proc. EARSel Workshop on Remote Sensing and GIS Applications to Forest Fire Management*, pp. 49–52. University of Alcala de Henares, Spain.
10. Hudak A.T., Brockett B.H. and Wessman C.A. (1998). Fire scar mapping in a southern African savanna. In *Proc. International Geoscience and Remote Sensing Symposium*, Seattle, WA. CD-ROM.
12. Patterson M.W. and Yool S.R. (1998). Mapping fire-induced vegetation mortality using Landsat Thematic Mapper data: a comparison of linear transformation techniques. *Remote Sens. Environ.* **65**, 132–142.
14. Cochrane M.A. and Souza C.M. (1998). Linear mixture model classification of burned forests in the eastern Amazon. *Int. J. Remote Sens.* **19**, 3433–3440.
15. Boardman J.W. and Kruse F.A. (1994). Automated spectral analysis: a geological example using AVIRIS data, North Grapevine Mountains, Nevada. In *Proc. ERIM Tenth Thematic Conference on Geologic Remote Sensing*, pp. 1407–1418. Environmental Research Institute of Michigan, Ann Arbor, MI.
16. Kraus T. and Samimi C. (2002). Biomass estimation for land use management and fire management using Landsat-TM and -ETM+. *Erdkunde* **56**(2), 130–144.
17. Huang, C., Wylie, B., Homer, C., Yang, L. and Zylstra, G. (2002). A Tasselled Cap Transformation for Landsat 7 ETM+ At-Satellite reflectance. *Int. J. Remote Sens.* **23**, 1741–1748.
18. Roy D.P. and Landmann T. (in press). Characterizing the surface heterogeneity of fire effects using multi-temporal reflective wavelength data. *Int. J. Remote Sens.*
19. Holben B.N., Eck T.F., Slutsker I., Tanre D., Buis J.P., Setzer A., Vermote E., Reagan J.A., Kaufman Y., Nakajima T., Lavenu F., Jankowiak I. and Smirnov A. (1998). AERONET — A federated instrument network and data archive for aerosol characterization. *Remote Sens. Environ.* **66**, 1–16.
20. Gertenbach W.P.D. (1983). Landscapes of the Kruger National Park. *Koedoe* **26**, 9–121.